

Single-Molecule Analysis of Genome Uncoating from Individual Human Rhinovirus Particles, and Modulation by Antiviral Drugs

Alejandro Valbuena,* Klara Strobl, Juan Carlos Gil-Redondo, Luis Valiente, Pedro J. de Pablo, and Mauricio G. Mateu*

Infection of humans by many viruses is typically initiated by the internalization of a single virion in each of a few susceptible cells. Thus, the outcome of the infection process may depend on stochastic single-molecule events. A crucial process for viral infection, and thus a target for developing antiviral drugs, is the uncoating of the viral genome. Here a force spectroscopy procedure using an atomic force microscope is implemented to study uncoating for individual human rhinovirus particles. Application of an increasing mechanical force on a virion led to a high force-induced structural transition that facilitated extrusion of the viral RNA molecule without loss of capsid integrity. Application of force to virions that had previously extruded the RNA, or to RNA-free capsids, led to a lower force-induced event associated with capsid disruption. The kinetic parameters are determined for each reaction. The high-force event is a stochastic process governed by a moderate free energy barrier ($\approx 20 \text{ kcal mol}^{-1}$), which results in a heterogeneous population of structurally weakened virions in which different fractions of the RNA molecule are externalized. The effects of antiviral compounds or capsid mutation on the kinetics of this reaction reveal a correlation between the reaction rate and virus infectivity.

1. Introduction

Viruses are nanomachines that can use energy to undergo controlled structural rearrangements required for host cell infection and viral multiplication.^[1–4] Genome uncoating is a crucial step in the infectious cycle of any virus and, thus, an important target for developing antiviral drugs. Uncoating involves the exposure to the host cell machinery of the genome initially contained in the virion.^[3,5–7] Different viruses accomplish this step using different strategies. For example, tailed bacteriophages (Caudovirales) inject their DNA genome into the cell. In contrast, human or animal non-enveloped viruses enter the host cell where they undergo one or several structural rearrangements that mediate the exposure and release of their nucleic acid genome. Depending on the virus, those rearrangements involve either the disassembly of the viral capsid, or the opening of a hole or channel in the capsid through which certain viral components, and ultimately the viral nucleic acid molecule, are translocated.^[5–7]

Human rhinovirus (HRV)^[8,9] is an important and widespread respiratory virus.^[10] The COVID-19 crisis has underscored the constant threat and dramatic health and socioeconomic consequences of infection by highly transmissible viruses of the respiratory tract.^[11] HRVs are responsible for most common colds which lead to countless lost work and school hours and huge economic losses each year. Moreover, HRV infections are related to or exacerbate severe, potentially lethal respiratory diseases including cystic fibrosis, asthma, bronchiolitis in children, and fatal pneumonia in elderly or immunocompromised adults.^[10,12–14] HRVs also exacerbate chronic obstructive pulmonary disease^[10,12,14] which, according to the World Health Organization, is the 3rd leading cause of death worldwide (with 3.23 million deaths in 2019). Several organic compounds have been identified that inhibit HRV infection of human cells by interfering with the uncoating of its RNA genome,^[15–18] but no anti-HRV drug has been approved yet.

HRV belongs to the Enterovirus genus within the Picornavirus family. In the HRV virion^[19] (Figure 1), the genomic

A. Valbuena, J. C. Gil-Redondo, L. Valiente, M. G. Mateu
Centro de Biología Molecular "Severo Ochoa" (CSIC-UAM)
Universidad Autónoma de Madrid
28049 Madrid, Spain
E-mail: avalbuena@cbm.csic.es; mgarcia@cbm.csic.es
K. Strobl, P. J. de Pablo
Departamento de Física de la Materia Condensada
Universidad Autónoma de Madrid
28049 Madrid, Spain
P. J. de Pablo
Instituto de Física de la Materia Condensada (IFIMAC)
Universidad Autónoma de Madrid
28049 Madrid, Spain

The ORCID identification number(s) for the author(s) of this article can be found under <https://doi.org/10.1002/sml.202304722>

© 2023 The Authors. Small published by Wiley-VCH GmbH. This is an open access article under the terms of the Creative Commons Attribution-NonCommercial-NoDerivs License, which permits use and distribution in any medium, provided the original work is properly cited, the use is non-commercial and no modifications or adaptations are made.

DOI: 10.1002/sml.202304722

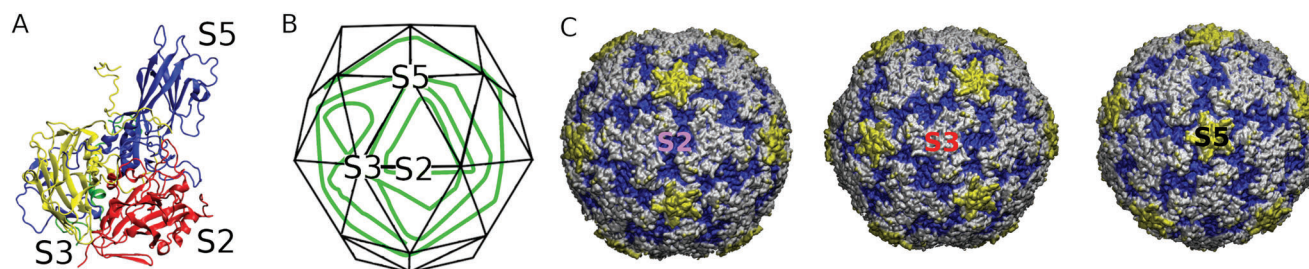


Figure 1. Structure of the HRV-B14 virion. A) ribbon representation of the HRV-B14 capsid protomer formed by one copy of each capsid protein: VP1 (blue), VP2 (red), VP3 (yellow), and VP4 (green). B) Schematic icosahedral architecture of the HRV virion. A green ribbon represents the internal, mostly disordered RNA molecule. C) Surface representation of the atomic structure of the HRV-B14 virion (PDB ID: 4RHV), color-coded from blue to yellow as a function of increasing radial distance, and observed along a twofold (S2) (left image), a threefold (S3) (center image) or a fivefold (S5) (right image) icosahedral symmetry axis. In all panels, the location of capsid icosahedral symmetry axes is indicated by labels: S2, S3, and S5.

single-stranded (ss) RNA molecule is surrounded by a naked (nonenveloped) icosahedral capsid 30 nm in diameter. The HRV capsid is composed of 60 identical hetero-oligomeric subunits (protomers), each formed by one copy of 3 proteins (VP1, VP2, VP3) and one extended, internally located polypeptide (VP4) (Figure 1A). During the morphogenesis of enteroviruses, pentameric subunits made of 5 protomers are assembled first, and 12 pentamers then coassemble with the genomic ssRNA molecule to form the virion^[20] (Figure 1B,C). HRV infects a host cell by binding a specific receptor on the cell surface, followed by internalization of the viral particle and uncoating of its RNA genome in a cell endosome.^[8,9]

Uncoating of the ssRNA genome of HRVs, polioviruses, and other species of enteroviruses has been studied using bulk techniques (reviewed in refs. [5,21–27]). Two discrete steps were identified: i) a structural transition of the virion (sedimentation coefficient ≈ 160 S for poliovirus or ≈ 150 S for HRV), that resulted in the release of VP4 subunits and the externalization of VP1 N-termini (Nt). This transition yielded an intermediate that still contains viral RNA (“A particle”, sedimentation coefficient ≈ 135 S for poliovirus or ≈ 120 S for HRV); and ii) extrusion of the RNA molecule through one of the pores that are transiently opened in the viral particle, that left a rearranged, empty capsid (sedimentation coefficient ≈ 80 S) as a byproduct. Both in HRV and poliovirus the openings occur at the centers of the interfaces between pairs of neighboring pentamers, where twofold capsid symmetry axis are located (one of them is labeled S2 in Figure 1).^[28–30]

Single-molecule techniques such as optical tweezers^[31–33] and atomic force microscopy (AFM)^[34,35] are being increasingly used to manipulate individual virus particles one at a time. These techniques, together with theoretical models and simulations, are providing deeper quantitative insights into virus structure, physical properties, and biological function within the rapidly growing field of physical virology.^[4,36–39] Bacteriophage nucleic acid packaging^[40,41] or ejection,^[42–44] interaction with cell receptors, cell entry and disassembly of eukaryotic viruses,^[45–49] virus morphogenesis,^[50–52] and virus biomechanics^[34,35,42,46,48,49,53–62] are being experimentally investigated at the single-particle level. However, single-particle studies of virus structural rearrangements involved in genome uncoating are scarce. Single-particle studies have already largely contributed to understand dsDNA ejection from tailed phages as driven by a high inter-

nal pressure inside a mechanically robust capsid.^[42–44] Single-particle studies of adenovirus uncoating^[6,7] revealed that viral particle disassembly and dsDNA release are partly controlled by internal pressure modulation.^[49] Uncoating of picornaviruses and parvoviruses has been the subject of structural and/or biochemical studies, and the release of the viral RNA from individual HRV virions^[61] or of the ssDNA from individual minute virus of mice virions^[62] has been visualized by AFM.

Single-molecule force spectroscopy (SMFS) in particular holds great potential for studying physical transitions of virus particles at the single-molecule level, including those associated with genome uncoating. SMFS has previously been used to investigate the directional unfolding of individual protein molecules. Protein unfolding analysis based on bulk experiments typically uses thermal or chemical energy to promote the reaction, and the values of the thermodynamics or kinetic parameters in the absence of the promoting agent are obtained by extrapolation.^[63] In SMFS pulling experiments on protein unfolding, the required energy is provided by mechanically stretching individual folded protein molecules.^[64–70] The values obtained for thermodynamic or kinetic parameters are then extrapolated to zero mechanical force.^[70]

In the present work, we have implemented a SMFS procedure to analyze the kinetics of structural transitions of single virus particles that involve either uncoating of the nucleic acid molecule or disassembly of the viral capsid. In these SMFS pushing experiments, an AFM instrument is operated under a force ramp (FR) protocol. The AFM cantilever is used to apply an increasing mechanical load on virus particles one at a time. Using HRV as a virus model, a transition was observed at a higher force that facilitated RNA exposure and release without capsid disruption. This transition preceded a second transition that was observed at lower force and involved the collapse of the viral capsid. The kinetic parameters of the two separate transitions were quantified for many individual virus particles. The results validated SMFS as an excellent approach to analyze, at the single-particle level, structural rearrangements of virus particles. Once validated, SMFS was used here to investigate a possible correlation between the effects of genetic mutation or capsid-binding compounds in the kinetics of the transition that facilitates RNA uncoating from the HRV virion, and impaired virus infectivity.

2. Results

2.1. Successive Mechanical Force Gradients Induce Two Distinct Physical Changes in Individual HRV Virions

Purified HRV-B14 ssRNA-filled virions (Figure S1A, Supporting Information) were subjected to a force gradient by indentation with the AFM tip (see Experimental Section). Virions were first adsorbed onto a mica substrate. However, adsorption to mica was weak, and many viral particles moved when subjected to relatively high force (up to 5 nN), which led to inefficient acquisition of data for statistical analysis. To reduce the slippage of viral particles under mechanical load, a functionalized solid surface to which the viral particles were covalently attached was used. AFM imaging showed that the covalently attached virions preserved the shape, overall dimensions, and visible surface features compared to virions that were adsorbed to mica without any covalent linkage (Figure S2, Supporting Information). Specifically, the same salient topographic features were observed in covalently attached virions ($N = 31$) and in adsorbed virions ($N = 9$) (Figure S2A,B, Supporting Information). Also, height distributions for individual virions (Figure S2C, Supporting Information) gave an average height for the covalently attached virions of 30.8 ± 0.9 nm ($N = 31$), a value indistinguishable from that obtained for virions adsorbed to mica, 30.8 ± 0.6 nm ($N = 9$), and in agreement with the virion diameter reported in Viperdb^[71] (32 nm).

Individual virus particles on the substrate were localized by wide-field AFM imaging. Once an isolated virion was localized, a narrow-field image was recorded to assess its physical integrity (by determining height and morphology; Figure 2A). Then, a variable mechanical force was applied by indentation with the AFM tip on the center-top of the same virion, using an adapted FR protocol, and a force versus time plot was obtained (Figure 2B). After this first indentation cycle had been completed, a second image of the viral particle was recorded (Figure 2C). Then a second indentation using FR was performed, and a second forceversustime plot was obtained (Figure 2D). The physical effect of this second indentation cycle on the viral particle was checked by recording a third AFM image of the viral particle (Figure 2E). Morphological changes in the viral particle during the first or second indentation were detected by comparing AFM images of the same particle before the first indentation (Figure 2A), after the first indentation, and before the second indentation (Figure 2C), and after the second indentation (Figure 2E) as well as the corresponding particle heights (Figure 2F).

Application of a first force gradient on each of 110 HRV particles (Figure 2A) led in most cases (77 virus particles, 70%) to a physical event that occurred at a relatively high force (Figure 2B) and was associated with a structural modification of the viral particle. This event was detected as an instantaneous drop in the force exerted on the particle (seen as a “spike” in the force versus time curve shown in Figure 2B; see also Figure S3A, Supporting Information, top panel). The event was also detected as an abrupt jump in the evolution of the tip-viral particle separation as a function of time (step size ΔZ ; Figure S3A, Supporting Information, bottom panel).

Comparison of AFM images of individual virions taken before (Figure 2A) or after (Figure 2C) a high-force event revealed two different outcomes: i) in 57% of the cases (44 particles), the force

applied led directly to a broken particle, or to particle unbinding; ii) in the remaining 43% of the cases (33 particles), the high-force event did not involve any modification in height or gross morphology of the viral particle but generally led to the appearance of a substantial amount of previously unseen material ($\approx 2\text{--}4$ nm in height) adjacent to the indented viral particle (Figure 2C). All of these 33 HRV virions were further analyzed by SMFS as described next.

Application of a second force gradient to each of the 33 virions that withstood the first force gradient without breaking apart (Figure 2C) led to a distinct event that was also observed as a spike in the force versus time curve, but at a much lower force (Figure 2D; Figure S3B, Supporting Information, top panel) than the first event (Figure 2B; Figure S3A, Supporting Information, top panel). Again, the new event was also detected as an abrupt jump in ΔZ (Figure S3B, Supporting Information, bottom panel). This second event invariably involved the collapse and eventual breakage of the viral particle as determined by drastic morphological changes (Figure 2E) and a quite reduced height profile (Figure 2F). In the following paragraphs, we will use the terms “high-force” or “low-force” when referring to the first or second event. These two events observed with virions covalently attached to the substrate were equally observed when virions non-covalently adsorbed onto a mica substrate were subjected to force gradients.

2.2. The High Force-Induced Transition in HRV Virions Facilitates Exposure and Release of the Viral RNA

Different lines of evidence indicate that the physical change detected in individual HRV virions during the high-force events facilitates exposure and release of the viral RNA:

- i. RNA-filled virions and empty capsids devoid of RNA were compared in FR spectroscopy experiments. Empty capsids were obtained from a purified virion preparation. The viral RNA was released from the virions without capsid disruption by a combination of dialysis against a mildly acidic buffer and moderate heating for a limited amount of time. The empty capsids were separated from any remaining virions by ultracentrifugation in sucrose gradients, and the actual presence of empty capsids in the fraction corresponding to particles with the expected sedimentation coefficient (80 S) was confirmed by negative staining transmission electron microscopy (see Experimental Section) (Figure S1B, Supporting Information). The empty capsids were adsorbed onto mica and subjected to FR (Figure 3) as described above for virions. Indentation of 21 individual empty capsids (Figure 3A) invariably resulted in a single, low-force event (Figure 3B) that involved a dramatic collapse of the viral particle (Figure 3C), partly revealed by a strong reduction in height (Figure 3D). Many virions adsorbed to mica under exactly the same conditions used for the empty particles showed high force events (Figure S3C, Supporting Information), whereas the empty particles invariably showed low force events only (Figure S3D, Supporting Information). Importantly, the force involved in the disruption of capsids chemically devoid of RNA was very similar to the force involved in the disruption of virions that had already undergone a first (high-force) transition

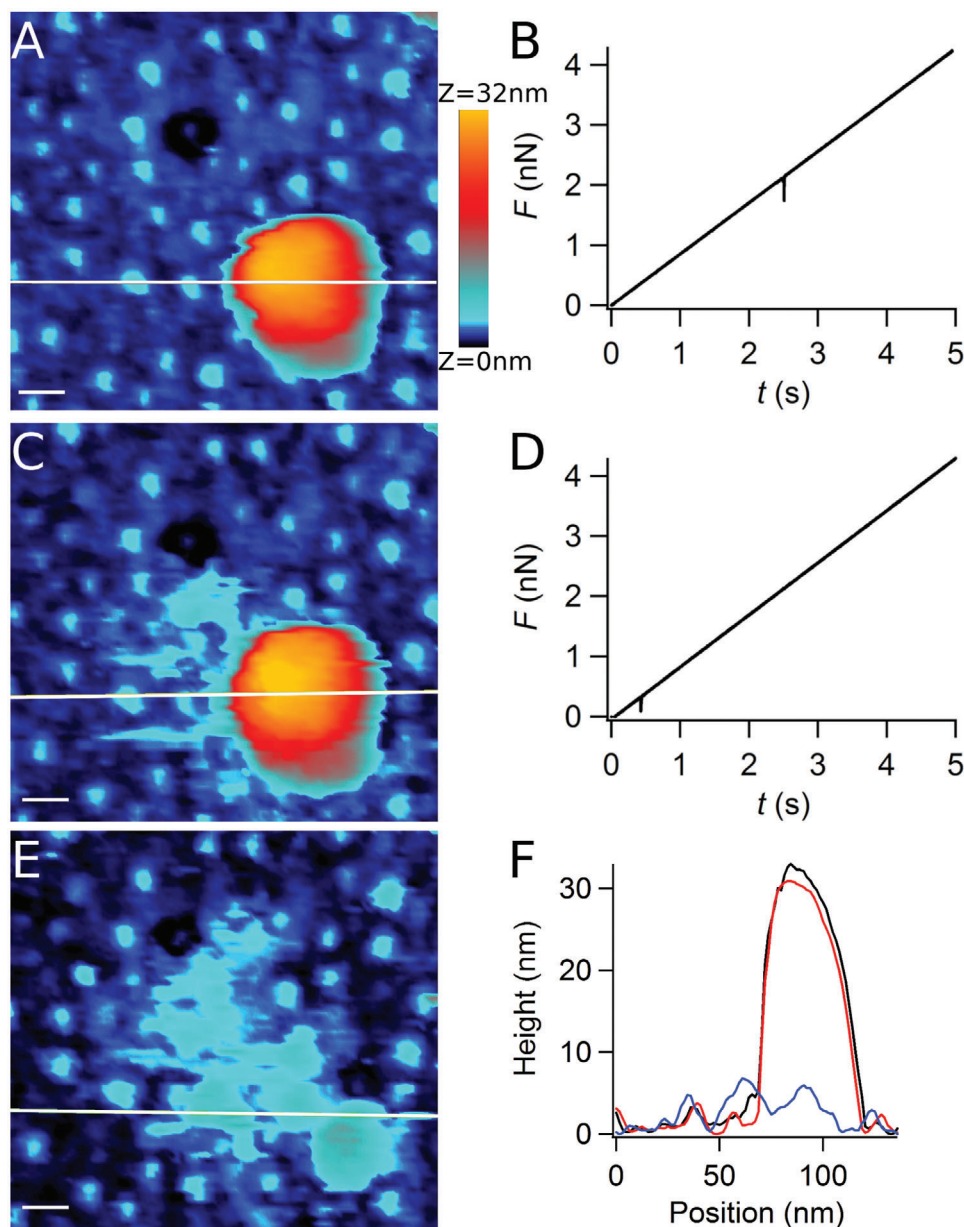


Figure 2. Mechanically induced physical events in an individual HRV virion using FR spectroscopy. A) AFM image of an intact virion before being indented by the AFM tip. B) Force versus time plot obtained during a first FR indentation of the viral particle. C) AFM image of the same virion after the first FR indentation. D) Force versus time plot obtained during a second FR indentation of the same viral particle. E) AFM image of the same virion after the second FR indentation. In panels (A,C,E) scale bars (15 nm) are included, and images are color coded in height (z) according to the scale represented at the center top of the figure. F) Topographic profiles obtained following the horizontal white traces indicated in the images shown in panels A (red), C (black), or E (blue). In panels (A,C,E) and any other AFM image in this study, particulate material with small size and low height (small pale blue dots) likely correspond to molecules of the reagent used to functionalize the surface, either free or bound to small contaminants or broken virus particle fragments present in the virus preparations.

(Table 1). Thus, virions that underwent a high-force transition were structurally weakened and, when they were again subjected to mechanical force, they behaved like capsids devoid of viral RNA.

- ii. After a high-force event during the first indentation of a virion, the viral particle essentially preserved its shape and approximate dimensions. However, for 31 of the 33 virions analyzed by SMFS, accurate height measurements could be

obtained that revealed a slight radial expansion (2.2% on average; Figure S4, Supporting Information). A quantitatively similar radial expansion of HRV particles was detected after they had uncoated their RNA in response to (bio)chemical cues in bulk experiments.^[72]

- iii. The new material visualized by AFM after a high-force event caused by the first indentation of a virion was invariably found in the immediate vicinity of the indented virus

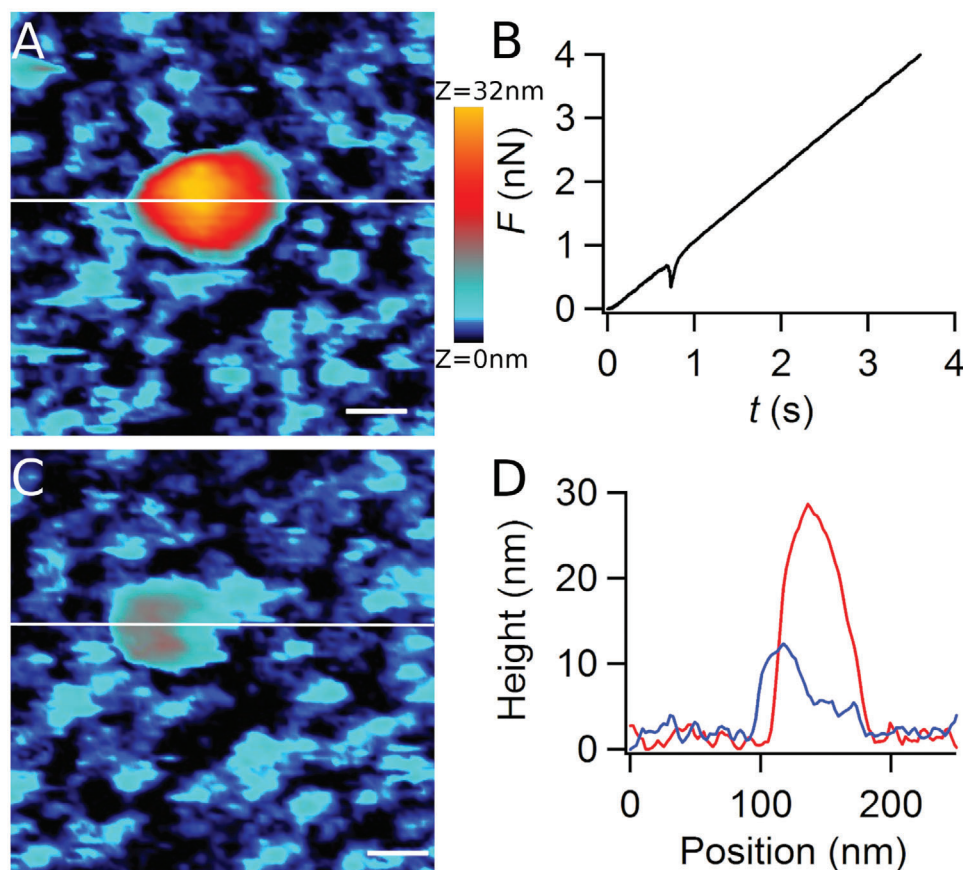


Figure 3. Mechanically induced physical events in an individual HRV empty capsid using FR spectroscopy. A) AFM image of an intact empty capsid before being indented by the AFM tip. B) Force versus time plot obtained during an FR indentation of the empty capsid. C) AFM image of the same empty capsid after the FR indentation. In panels (A) and (C) scale bars (30 nm) are included, and images are color-coded in height (z) according to the scale represented at the center top of the figure. D) Topographic profiles obtained following the horizontal white traces indicated in the images shown in panels (A) (red), or (C) (blue).

Table ^{a)}. Kinetic parameters for the transitions that either facilitated RNA release from the HRV virion or involved the disruption of the HRV capsid under different applied forces.

Particle ^{a)}	r [nN s ⁻¹]	#part	#rel	N_{events}	RNA uncoating				Capsid breaking			
					F_{high} [nN]	α_{OR} [s ⁻¹]	ΔG_R^\ddagger [kcal mol ⁻¹]	x_R^\ddagger [nm]	F_{low} [nN]	α_{OB} [s ⁻¹]	ΔG_B^\ddagger [kcal mol ⁻¹]	x_B^\ddagger [nm]
Virion	0.72 ± 0.05	36	11	47	2.1 ± 0.6	$(2.9 \pm 0.8) \times 10^{-3}$	19.4 ± 0.3	11.8 ± 0.6	0.4 ± 0.3	0.51 ± 0.11	16.4 ± 0.2	14 ± 2
	0.86 ± 0.06	38	12	50	2.0 ± 0.5	$(3.7 \pm 1.0) \times 10^{-3}$	19.3 ± 0.3		0.5 ± 0.3	0.30 ± 0.08	16.7 ± 0.3	
	1.0 ± 0.1	23	7	30	2.4 ± 0.4	$(1.4 \pm 0.5) \times 10^{-3}$	19.8 ± 0.4		0.6 ± 0.3	0.34 ± 0.09	16.6 ± 0.3	
	1.9 ± 0.2	13	3	16	2.8 ± 0.3	$(0.9 \pm 0.4) \times 10^{-3}$	20.1 ± 0.4		0.5 ± 0.2	0.82 ± 0.20	16.1 ± 0.2	
	Overall	110	33	143	NA	$(2.2 \pm 1.3) \times 10^{-3}$	19.6 ± 0.4		0.5 ± 0.3	0.49 ± 0.24	16.4 ± 0.5	
Capsid	1.2 ± 0.1	21	NA	21	NA	NA	NA	NA	0.5 ± 0.2	0.16 ± 0.03	17.0 ± 0.2	21 ± 2

^{a)} r , force rates; #part, number of particles analyzed; #rel, number of particles in which RNA release was detected; N_{events} , number of observed events; F_{high} , F_{low} , average force value for the high-force or the low-force event, respectively; α_{O} , reaction rate; ΔG^\ddagger , difference in free energy between the transition state and the initial state (either intact virion for the reaction that facilitates RNA release, or capsid for the disruption reaction); x^\ddagger , distance along the mechanical coordinate between the transition state and the initial state. Kinetic parameters of each reaction were calculated by fixing r for each experimental condition, linking x^\ddagger , and leaving α_{O} free for all the fittings. ΔG^\ddagger was calculated assuming a natural frequency of the process of $5 \times 10^{11} \text{ s}^{-1}$. NA, not applicable.

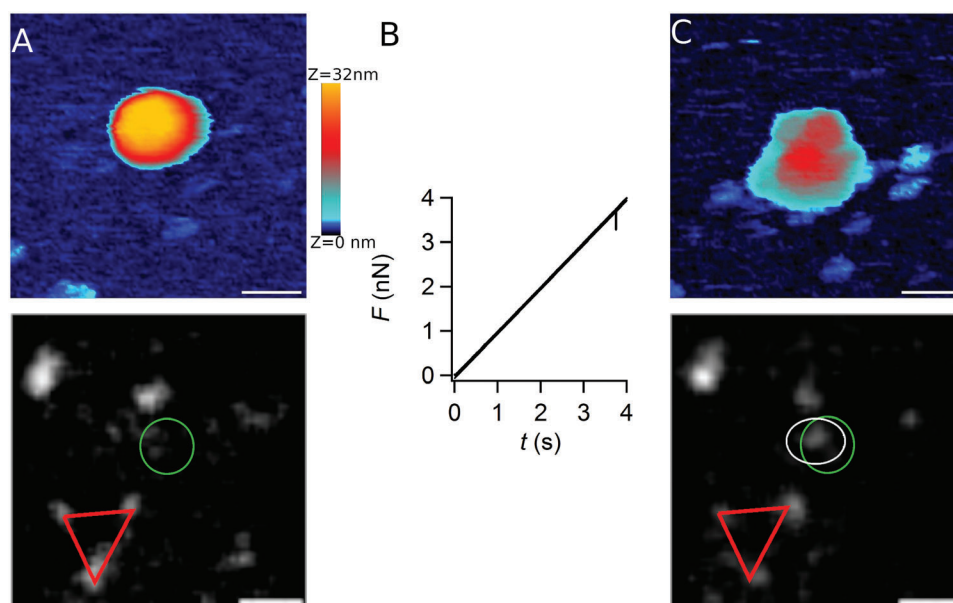


Figure 4. RNA exposure from HRV virions under mechanical load in FR spectroscopy experiments. A) An intact virion before being indented by the AFM tip. Up: a narrow-field AFM image of the selected virion. Bottom: a very wide-field fluorescence microscopy image of the area around the position of the indented virion. Fluorescent objects in the field serve as landmarks (three of them are highlighted with a red triangle). B) Force versus time plot obtained during an FR indentation of the viral particle. A high force-related event is observed. C) The same viral particle shown in panel (A) after a first indentation that resulted in a high force-related event. Up: AFM image. Bottom: fluorescence microscopy image. In the bottom images in panels (A) and (C), a green circle indicates the uncertainty in the actual position of the virus in the imaged field. A new fluorescent spot (indicated by a white circle) colocalized with the indented viral particle (green circle) within the positional error of the instrument. Small differences in intensity of some background fluorescence spots between the images in panels (A) or (B) are likely due to: i) minor fluctuations in signal propagation along the line of sight; ii) degradation of fluorophore-bound contaminating RNA in the sample. Neither of those effects may explain the large increase in brightness of the spot associated with the indented virion (white circle). Scale bars in AFM images are 50 nm. Scale bars in fluorescence microscopy images are 1 μm . AFM images are color-coded in height (z) according to the scale represented at the center top of the figure.

particle (Figure 2C), and not elsewhere. This observation suggests that some material had been released by the indented viral particle. As the material was invariably ejected without any detectable change in capsid morphology (Figure 2C) or reduction in height (Figure 2F), no release of capsid proteins VP1, VP2, and/or VP3 could be expected. The released material should correspond to the internally located viral RNA and/or VP4 molecules.

- iv. An instrument combining an atomic force microscope with a fluorescence microscope for single-molecule analysis^[73] was then used to determine whether at least part of the material released from the virion after the first, high-force transition corresponded to viral RNA. A fluorophore (Ribogreen) that strongly emits visible light upon binding to RNA was added to the medium, and individual virions were imaged by AFM and subjected to a force ramp as described above. The (x,y) coordinates of the indented virus on the substrate were estimated by AFM imaging. The (x,y) coordinates of any fluorescence spot that appeared immediately after the virus particle was subjected to a force ramp were estimated by fluorescence imaging with the same combined instrument. **Figure 4** shows the result obtained with a single virion. Before indentation, no intense fluorescence spot was observed around the approximate position where the virion was located (green circle in Figure 4A). A first indentation of the virion produced a high-force event as expected (Figure 4B). After indentation, an intense fluorescence spot was clearly observed whose po-

sition (white circle) colocalized with that of the indented viral particle (green circle) within the instrumental error inherent to those measurements (Figure 4C). Thus, the high-force event did involve exposure of the viral RNA molecule to the environment.

The volume of the material released by 26 of the 33 HRV virions for which SMFS analysis revealed a high-force event was then estimated (**Figure 5**) by pixel-by-pixel subtraction of AFM images (Figure 5A). The presence of material outside of the imaged area prevented the adequate quantification of the material released by the other 7 particles analyzed by SMFS. As shown in Figure 5B,C, the average volume of the detected extruded material was variable. It peaked at $\approx 5000 \text{ nm}^3$ and reached up to $\approx 10\,500 \text{ nm}^3$. This volume was compared to those of the HRV RNA molecule or the HRV capsid proteins. As the volume of a nucleic acid molecule adsorbed on a solid surface may be slightly different than its volume in solution, the volume of the HRV RNA molecule was estimated from previous results obtained by AFM imaging of a ss nucleic acid adsorbed on a solid substrate in liquid.^[74] The estimated volume of the full-length HRV-B14 ssRNA (7200 nucleotides) under these conditions was $\approx 9300 \text{ nm}^3$. The volumes of protein molecules of different molecular weights had also previously been determined by AFM imaging in liquid.^[75] The estimated volume of the HRV-B14 capsid proteins under these conditions was $\approx 54 \text{ nm}^3$ for VP1, VP2, or VP3, and $\approx 15 \text{ nm}^3$ for VP4.

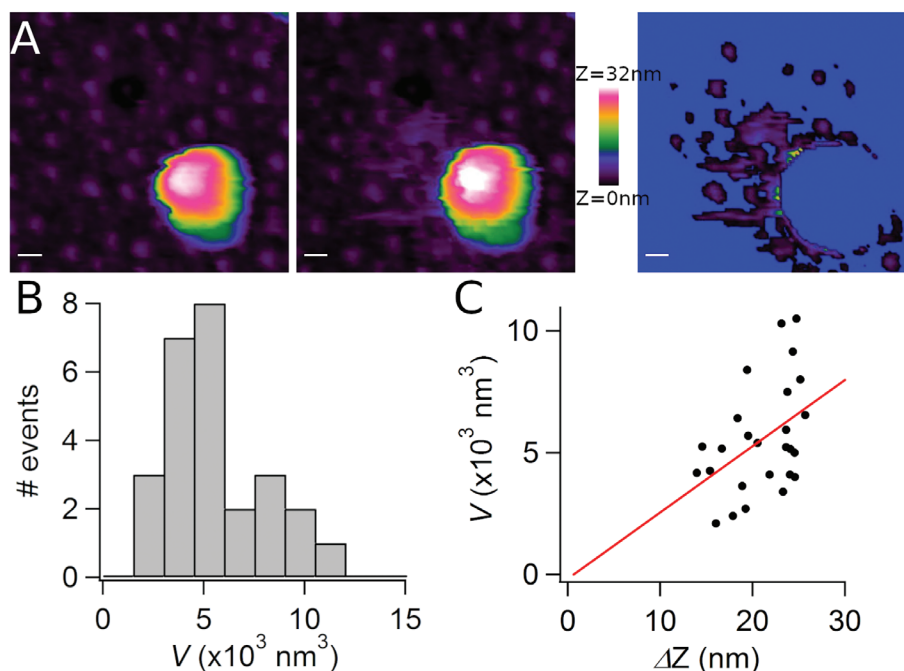


Figure 5. Volumetric analysis of the material extruded from an HRV virion under mechanical load in an FR spectroscopy experiment. The analysis corresponds to the same viral particle shown in Figure 2. A) A virus particle before (left) or after (center) some material was extruded in a high-force event. These images correspond to those shown in Figure 2A,C, but here they were colored in height (z) using a different code to highlight small height differences (color scale is shown on the right side of those images). The image at right is a different image obtained by pixel-by-pixel subtraction of the image at left (before indentation) from the image at the center (after indentation). B) Distribution of the volume of material extruded from 26 individual virions during high-force events. C) Approximate volume of material extruded from those virions as a function of ΔZ (the tip-sample separation jump). Linear fitting of these data (red line) yielded a correlation coefficient $R = 0.44$.

If all 60 VP4 molecules in an HRV virion had been released and immobilized onto the surface, they would occupy a volume of $\approx 900 \text{ nm}^3$ (only $\approx 9\%$ of the maximum detected extruded material volume). If the entire RNA molecule had been released and immobilized onto the surface, it would occupy a volume of $\approx 9300 \text{ nm}^3$ ($\approx 89\%$ of the maximum detected extruded material volume) (Figure 5C). These estimations, taken together with the evidence that the high-force event involved RNA exposure to the environment (points i to iv above), indicate that the vast majority of the material released by indented virions and adsorbed onto the substrate corresponds to viral RNA, with perhaps a minor fraction corresponding to capsid proteins (VP4).

For most virus particles that had undergone a high-force transition, at least half of the RNA molecule may have been extruded from the capsid (peak of the histogram in Figure 5B). In some cases, the RNA molecule may have been fully externalized, consistent with the highest amount of material detected around the particle (Figure 5B). The plot represented in Figure 5C revealed that the volume of the material extruded from a single virion (mainly RNA as supported by the evidence described above) increased with the magnitude of ΔZ in the corresponding force-related event (determined from tip-sample separation versus time plots such as those in the bottom line of Figure S3, Supporting Information). Linear fitting of extruded volume versus ΔZ yielded a limited correlation coefficient ($R = 0.44$).

These observations indicate that the cantilever tip worked in these experiments like a sort of “molecular pimple squeezer”. The application of a high enough mechanical force induced first

a structural transition that enabled the subsequent release of the RNA molecule out of the viral particle, facilitated by the increasing load being applied. The pH-induced release of RNA from individual HRV virions had previously been imaged by AFM.^[61] In our experiments, mechanical force on individual virions substituted acidification as a promoting agent for viral RNA release.

To sum up, the high-force event observed when individual HRV virions were subjected to a first indentation in FR experiments corresponds to a mechanically induced structural transition of the viral particle that facilitates extrusion of the HRV genome molecule. The energy required for triggering this transition, which can be supplied *in vivo* or *in vitro* through receptor binding, acidification, or heating, can also be supplied *in vitro* by the application of mechanical force. This finding opened up the possibility of quantitatively determining by FR spectroscopy the kinetic parameters of the structural transition of individual virus particles associated with the uncoating of its single genomic nucleic acid molecule (see below).

2.3. The Viral RNA Strengthens the HRV Virion

In FR experiments, the physical integrity of RNA-filled HRV virions was preserved until they were subjected to a relatively high force ($\approx 2 \text{ nN}$ under the tested conditions). After that event, the viral particles typically externalized a part of all of their RNA. These particles behaved in FR experiments like HRV capsids that had been fully devoid of RNA by chemical means, both

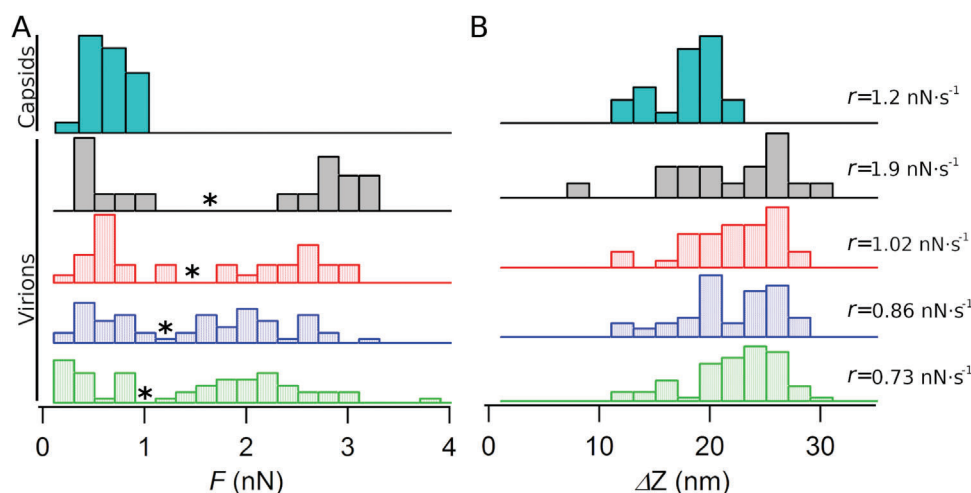


Figure 6. Normalized distribution of high-force and low-force physical events triggered on individual HRV particles by applied force gradients. A) Force (F) histograms. B) Jump size (ΔZ) histograms. The total area of the bars in each histogram has been normalized to the same value to facilitate comparison. Thus, in each histogram, the relative height of a bar represents the relative frequency of events that occurred at a given value of F or ΔZ relative to the frequencies of events that occurred at other F or ΔZ . The upper histograms (cyan bars) correspond to empty capsids at a r value = $1.2 \pm 0.1 \text{ nN s}^{-1}$. All other histograms correspond to virions at different r values (grey, $r = 1.9 \pm 0.2 \text{ nN s}^{-1}$; red $r = 1.02 \pm 0.07 \text{ nN s}^{-1}$; blue $r = 0.86 \pm 0.06 \text{ nN s}^{-1}$; green $r = 0.73 \pm 0.05 \text{ nN s}^{-1}$). Average F values for each of the populations observed (low-force population only for empty capsids, low-force and high-force populations for virions) are indicated in Table 1. In panel (A), an asterisk denotes a minimum in the force value that separates the high-force events from the low-force events.

types being disrupted by the application of the same low force ($\approx 0.5 \text{ nN}$ under the tested conditions) (disruption force values F for both types of particles are indicated in Table 1). Thus, the viral RNA molecule strengthens the HRV virion relative to the viral capsid.

2.4. Statistical Analysis of High-Force and Low-Force Physical Events Triggered on Individual HRV Particles by Applied Force Gradients

To quantify the kinetics of the HRV structural transitions triggered by force gradients, it was necessary to determine first the exact forces at which each event occurred, using many individual virus particles and different force rates. Only events that involved relatively large ΔZ jumps corresponding to a sizable fraction of particle diameter could correspond to the substantial structural changes in the particle required for either RNA release or particle breakage. During indentation minor events involving small ΔZ jumps were sometimes detected in addition to high-force or low-force events involving large ΔZ jumps. Those minor events were likely caused by some sliding of the AFM tip on the virion surface or small shifts in the orientation/inclination of the viral particle attached to the surface. Thus, for the analysis of high-force or low-force events respectively associated with RNA release from the virion or capsid breakage, only events with a ΔZ value $\geq 30\%$ of the particle height ($\approx 10 \text{ nm}$) were considered. Force histograms (Figure 6; Figure S5, Supporting Information) were obtained from FR experiments using either a total of 110 particles from virion preparations or 21 particles from preparations of empty capsids chemically devoid of RNA. Each histogram included all significant events (ΔZ jump $\geq 30\%$ of the particle height) registered when indenting many individual viral parti-

cles. For particles in empty capsid preparations, only one population of events (low force) was observed (upper histogram in Figure 6A). In contrast, for particles in virion preparations, two clearly separate populations of events (low force and high force) were observed (Figure S5A, Supporting Information, and all histograms but the upper histogram in Figure 6A). During the first indentation, most events were high-force (related to RNA uncoating) (right peak in Figure S5A, Supporting Information). Some low force events were also observed (left peak in Figure S5A, Supporting Information), which likely corresponded to virions that had been pre-empted of RNA during purification and storage, a well-known occurrence for HRV. During the second indentation of virions, all events were low-force (related to the collapse of the viral capsid). For every single virion, the second event occurred at a lower force than the first event. For virions, force averages were separately calculated for the two populations at each tested r . For high-force events the required average force increased linearly with r ; in contrast, for low-force events, the required average force was not dependent on r (compare in Table 1 the force values obtained for virions or capsids at different rates; see also Figure S6A, Supporting Information).

Step size ΔZ (jumps in tip-viral particle separation) associated with the high-force or low-force events was also represented in histograms (Figure 6B). Each ΔZ histogram included jump events registered when indenting many individual viral particles at a specific r . For empty capsids, the ΔZ histogram (upper histogram in Figure 6B) revealed only one population with an average $\Delta Z = 17 \pm 3 \text{ nm}$. For virions, the ΔZ histograms (all but the upper histogram in Figure 6B) revealed a single population with an average $\Delta Z = 21 \pm 3$, slightly larger than that obtained for empty capsids. This difference may be due to the higher deformability of empty capsids relative to virions before the force event occurs.

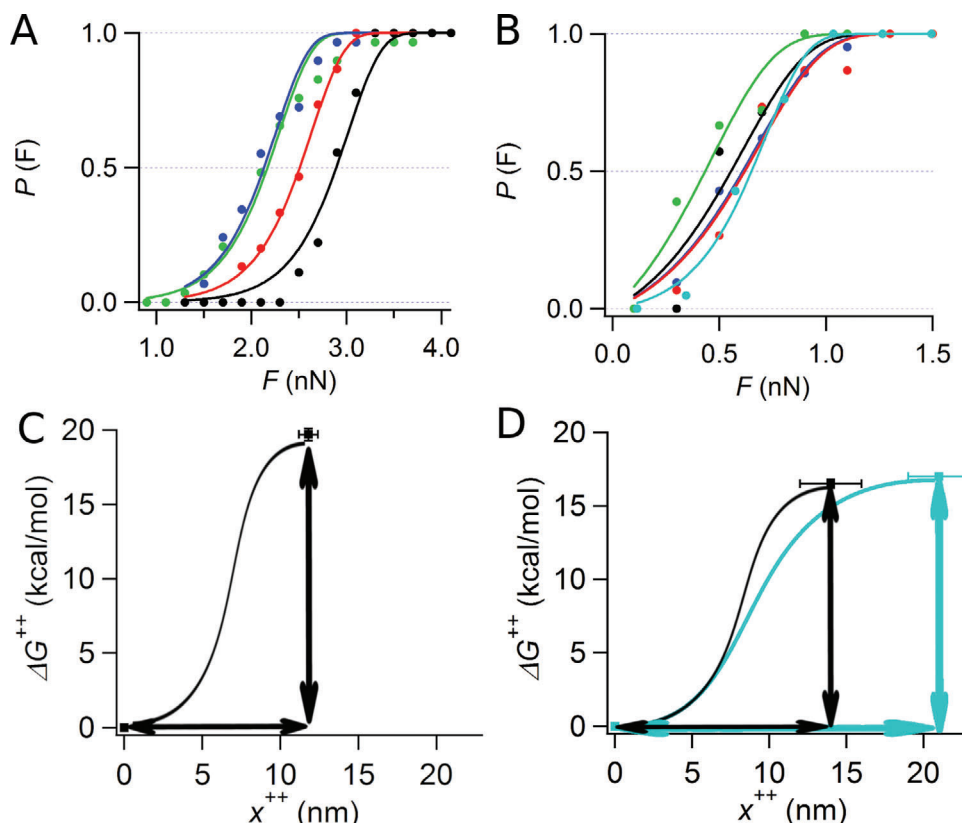


Figure 7. Calculation of kinetic parameters for the high-force transition that facilitated RNA release or low-force transition that involved capsid disruption. A,B) normalized experimental P_u values as a function of F at different r (circles) and their fitting (continuous lines) to a two-state model of the high-force transition (RNA release) (A), or the low-force transition (capsid breakage) (B). In panels A and B, the data and fitting curve obtained for virions at different r values are colored green ($r = 0.74 \text{ nN s}^{-1}$), blue ($r = 0.86 \text{ nN s}^{-1}$), red ($r = 1 \text{ nN s}^{-1}$) or black ($r = 1.9 \text{ nN s}^{-1}$). The data and fitting curve obtained for capsids devoid of RNA are colored cyan ($r = 1.2 \text{ nN s}^{-1}$). Fitting was performed by leaving α_0 free, linking x_R^{\ddagger} , and fixing r to the experimentally determined force rates ($\chi^2 = 0.16$ and $\chi^2 = 0.09$ for fittings in A and B respectively). C,D) Representation of the free energy difference between the initial state (at $x^{\ddagger} = 0$) and the transition state \ddagger for the high-force transition (C) or the low-force transition (D). In panels (C) and (D) the distance between the initial state and the transition state x_0^{\ddagger} , and the free energy barrier of the reaction ΔG^{\ddagger} , are respectively indicated by horizontal and vertical arrows. In panel (D), black or cyan curves and arrows respectively correspond to capsids that resulted from either mechanical or chemical RNA release from virions. Error bars in ΔG^{\ddagger} calculated by error propagation were too small to be visible in the plot represented in panel (D). The curves depicted in panels (C) and (D) are there for illustrative purposes only, and are not derived from the actual data.

To sum up, statistical analysis of FR recordings obtained with many individual HRV particles confirmed some qualitative features and revealed additional, quantitative features of the physical events that resulted from the application of mechanical force on individual HRV particles. i) higher-force events always preceded lower-force events, consistent with their physical interpretation: a transition that facilitated RNA release from the virion at higher force, followed by the collapse of the emptied viral capsid at lower force; ii) the force required to trigger high-force events increased with r , whereas the force required to trigger low-force events was not dependent on r .

2.5. Kinetic Parameters of the Transitions of Individual HRV Particles that Facilitated RNA Release or Involved Capsid Breakage, Quantified by FR Spectroscopy

The kinetic parameters of the structural transition that facilitated RNA release from the HRV virion, and those corresponding to

the subsequent collapse of the viral particle, were determined by considering two-state reactions. In a high-force event, the initial state is the intact virion and the final state is a structurally rearranged viral particle that is prone to RNA release. In a low-force event, the initial state is the rearranged viral capsid and the final state is the disrupted capsid.

The variation in applied force over time was precisely controlled by the feedback loop in the AFM setup and was a known parameter. From this parameter, the variation in energy supplied to the system was determined, which allowed a calculation of the probability of observing a particular physical event (P_u). More specifically, P_u as a function of the applied force (F) was determined by directly integrating the force histograms (Figure 6A; Figure S6B, Supporting Information). An operative threshold of 1–1.5 nN was chosen, and the values obtained for forces above or below this threshold (indicated by asterisks in Figure 6A) were separately re-normalized. In this way, P_u as a function of F was separately obtained for high-force events (Figure 7A), and for low-force events (Figure 7B).

Table 2. Kinetic parameters for the transition that facilitated RNA release from the HRV virion in the absence or presence of antivirals or a capsid mutation..

Virus ^{a)}	r [nN s ⁻¹]	#part	#rel	%	N_{events}	α_{OR} [s ⁻¹]	ΔG_R^\ddagger [kcal mol ⁻¹]	x_R^\ddagger [nm]
wt	0.86 ± 0.06	38	12	37	50	$(11 \pm 3) \times 10^{-3}$	18.6 ± 0.3	9.3 ± 0.7
wt + pirodavis	0.87 ± 0.06	24	7	38	31	$(4.8 \pm 1.8) \times 10^{-3}$	18.7 ± 0.4	10 ± 1
wt + pleconaril	0.84 ± 0.08	14	5	36	19	$(2.4 \pm 1.4) \times 10^{-3}$	19.4 ± 0.6	17 ± 2
R3143A	0.87 ± 0.02	18	3	44	21	$(0.23 \pm 0.14) \times 10^{-3}$	19.8 ± 0.6	15 ± 1

^{a)} wt, wild-type HRV-B14; R3143A, HRV-B14 mutant R3143A; #part, number of particles analyzed; #rel, number of particles for which RNA release was detected; N_{events} , number of events; α_{OR} , natural reaction rate; ΔG_R^\ddagger , difference in free energy between the transition state and the initial state (intact virion); x_R^\ddagger , distance along the mechanical coordinate between the transition state and the initial state.

P_u depends on three parameters related to the kinetics of the physical event being analyzed, as given by Equation (1) (see Experimental Section): the rate constant of the reaction (α_0), the distance from the initial state to the transition state of the reaction (x^\ddagger), and the rate at which the applied force is increased (r), which is the independent variable that was modified on purpose in order to minimize the degeneracy when obtaining kinetic parameters. By simultaneous fitting of experimental P_u values obtained from either high-force or low-force events at different r to Equation (1), the values of α_0 and x^\ddagger at each of the tested force rates were obtained. The free energy barrier of the process, that is, the free energy difference between the initial state and the transition state (ΔG^\ddagger) at each tested r was calculated from the corresponding rate constant (α_0) using Equation (2) and considering a natural frequency for the process of $5 \times 10^{11} \text{ s}^{-1}$.^[23] For calculation of the values of the relevant parameters α_0 , x^\ddagger and ΔG^\ddagger in the absence of applied force, the values obtained at different r values (from $r = 0.74$ to 1.9 nN s^{-1}) for virions, or at $r = 1.2 \text{ nN s}^{-1}$ for empty capsids, were used for a direct fit to a two-state model as described in the Experimental Section (Figure 7C,D).

The calculated values of the kinetic parameters (rate constant α_0 , position of the transition state along the reaction (mechanical) coordinate x^\ddagger , and activation free energy ΔG^\ddagger) are shown in Table 1. For the high-force events observed with virions (R subindex), the values extrapolated to the absence of applied force were $\alpha_{\text{OR}} = (2.2 \pm 1.3) \times 10^{-3} \text{ s}^{-1}$, $x_R^\ddagger = 11.8 \pm 0.6 \text{ nm}$ and $\Delta G_R^\ddagger = 19.6 \pm 0.4 \text{ kcal mol}^{-1}$. For the low-force events observed with viral particles that had already undergone a high-force event (B subindex), these values were $\alpha_{\text{OB}} = 0.49 \pm 0.24 \text{ s}^{-1}$, $x_B^\ddagger = 14 \pm 2 \text{ nm}$ and $\Delta G_B^\ddagger = 16.4 \pm 0.5 \text{ kcal mol}^{-1}$. For the low-force events observed with capsids chemically devoid of RNA, the values were $\alpha_{\text{OB}} = 0.16 \pm 0.03 \text{ s}^{-1}$, $x_B^\ddagger = 21 \pm 2 \text{ nm}$ and $\Delta G_B^\ddagger = 17.0 \pm 0.2 \text{ kcal mol}^{-1}$. These results are considered in the Discussion.

2.6. Quantitative Effects of Antiviral Drugs on the Kinetics of the Transition that Facilitated RNA Release from Individual HRV Virions

The FR spectroscopy procedure developed here to quantify kinetic parameters for the structural transition that facilitated RNA release from individual virions was used also to investigate whether the kinetics of this transition may have a role in virus survival. A proof-of-principle for such a relationship is provided here by quantitatively investigating the effects of two capsid

pocket-binding antiviral drugs (described next) or a deleterious point mutation (described below).

HRV-B14 virions were incubated with either pleconaril or pirodavis at concentrations that promoted binding to the virus particles and inhibited viral infection of cultured cells to different extents. Under the conditions used, pirodavis had a moderate inhibitory effect, whereas pleconaril had a stronger inhibitory effect.^[60] The parameters of the transition that facilitated RNA release from many drug-bound virions were determined by SMFS exactly as described above for drug-free virions (Table 2). For these comparisons, a single r was used. Determination of the r values actually used confirmed they corresponded to virtually the same value (within 0.84 – 0.87 nN s^{-1} , Table 2).

P_u values as a function of the applied force F for the transition in the absence or presence of either pleconaril or pirodavis are represented in Figure 8A. Fitting P_u values to Equation (1) yielded the values for α_{OR} and x_R^\ddagger . ΔG_R^\ddagger was calculated from the corresponding rate constant α_{OR} using Equation (2). The results (Figure 8B, Table 2) revealed that, under the conditions used, pirodavis had a moderate effect (twofold reduction) in the free energy barrier of the structural rearrangement that facilitated RNA release from the virion, the reaction rate, and the position of the transition state along the reaction mechanical coordinate. In contrast, pleconaril caused a fourfold reduction in the reaction rate by increasing the free energy barrier and shifted the position of the transition state from $x_R^\ddagger = 9.3 \text{ nm}$ to 15 nm (Table 2). To sum up, capsid pocket-binding anti-HRV drugs reduced to different extents the rate of the structural transition that facilitated RNA release from individual HRV virions, an effect that could be related to their antiviral action.

2.7. The Reaction Rate of the Transition that Facilitated RNA Release from Individual HRV Virions Correlates with Virus Infectivity

The results obtained using capsid pocket-binding antiviral drugs suggested the possibility of a linkage between a reduced rate of the HRV transition that facilitated RNA release, and impaired HRV infectivity. To challenge this hypothesis, a deleterious HRV mutant was also subjected to FR spectroscopy. This mutant (R3143A) differs from its parent virus (HRV-B14) in a single amino acid residue per capsid subunit, located close to each capsid twofold axis where the RNA exits the viral particle during viral genome uncoating. Any correlation between changes in reaction rate and viral infectivity that could be found when comparing

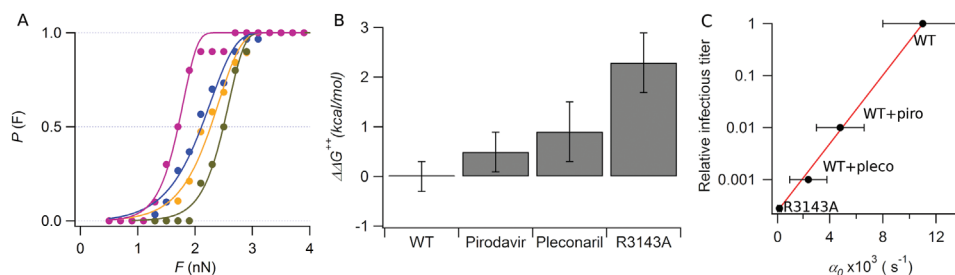


Figure 8. Quantitative effects of anti-HRV drugs and a mutation in the HRV capsid on the kinetics of the transition that facilitated RNA release, and correlation with reduced HRV infectivity. A) Normalized experimental P_u values as a function of F at a fixed r value (circles) and their fitting to a two-state model (lines) for HRV-B14 in the absence (blue) or the presence of either pirodavis (yellow) or pleconaril (purple), or for the HRV-B14 R3143A mutant in the absence of drug (green). Fitting was performed by leaving both α_0 and x_R^{\ddagger} free and fixing r to the experimentally determined force rates ($\chi^2 = 0.11$). B) Representation of the difference $\Delta\Delta G_R^{\ddagger}$ between the ΔG_R^{\ddagger} of the transition for the drug-bound or mutant virion and the ΔG_R^{\ddagger} for the wt virion in the absence of the drug. C) Plot of the relative infectious virus titers versus the reaction rates α_0 for the transition that facilitated RNA release under the same conditions, for HRV-B14 in the absence of drug (taken as reference, infectious titer normalized to a value of 1), HRV-B14 in the presence of either pirodavis (piro) or pleconaril (pleco), or the HRV-B14 R3143A mutant. Linear fitting of these values (red line) yielded a correlation coefficient $R^2 = 0.997$.

those quite different modifications (drug binding or mutation) had a higher chance of reflecting a true functional linkage.

Eighteen individual R3143A mutant virions were analyzed in FR spectroscopy experiments under the same conditions described above for analysis of comparable numbers of drug-free or drug-bound HRV-B14 virions, and the corresponding kinetic parameters for the reaction were obtained (Table 2). The results revealed that the deleterious mutation R3143A drastically reduced the reaction rate (almost by one order of magnitude) by increasing the free energy barrier of the reaction, and also shifted the position of the transition state (Table 2).

Then, the relative infectivity of drug-free, pirodavis-bound, or pleconaril-bound HRV-B14 virions and of mutant R3143A virions was plotted against the corresponding reaction rates. The results (Figure 8C) revealed an excellent quantitative correlation. This observation indicates that the rate of the structural rearrangement that facilitates the exit of the viral genome from the HRV virion may influence the efficiency of the infection process.

3. Discussion

Initiation of infection of a human or animal host by a virus is not a bulk event involving large numbers of virions and averaged molecular effects. There is ample evidence that relatively few virions typically enter the host organism compared to the very high number of infection-susceptible host cells.^[76] The extremely low multiplicity of infection (ratio between the number of infecting virion and the number of susceptible host cells) virtually ensures that most susceptible host cells are not infected, and a few cells will be infected by one virion only. During the initiation of infection, the probability of two or more virions entering the same host cell is close to zero. As virus populations are not genetically and phenotypically homogeneous,^[77] the outcome of a cell infection process critically depends on the particular traits of the single virion that happens to enter the cell; it will also depend on the stochasticity at the single-molecule level of the reactions that initiate infection, including genome uncoating. Such a scenario lends itself to single-molecule studies of those reactions to complement studies on the molecular processes involved in viral infection using bulk techniques.

The release of single nucleic acid molecules from individual virions in vitro had previously been visualized by AFM for different viruses^[44,46,62,78] including HRV.^[61] The reaction was triggered by treatments such as dehydration,^[78] acidification,^[61] or the application of mechanical force.^[44,46,62] Most of those approaches were not intended for quantitative kinetic analysis. However, in a remarkable study Kellermayer et al.^[44] determined the kinetic parameters of dsDNA ejection from bacteriophage T7, which is pressurized to tens of atmospheres. Tapping the T7 capsid wall with an oscillating AFM cantilever triggered the rapid ejection of the dsDNA molecule through the phage tail.

SMFS as implemented in the present study provides a general procedure to detect structural transitions of individual virus particles, and to quantify at the single-molecule level the kinetics of such transitions, including those involved in uncoating of the viral nucleic acid molecule. In conventional AFM indentation experiments, there is no feedback to control the rate at which energy is supplied to the system. This condition can be met by setting a constant force (force clamp), but using this mode drifts in force may occur if measurements have to be performed during a relatively long period of time, leading to artifacts. In the SMFS approach, the temporal evolution of the force (force ramp) is predetermined and controlled, and the acquisition of data requires less time, which minimizes the drifting of force. SMFS can be used irrespective of virus type, the presence or absence of pressure in the particle, the input energy required, or the mechanism involved. As a proof-of-principle, here we applied SMFS to study a transition of HRV virions associated with genome uncoating.

The mechanism of genome uncoating of HRV and other enteroviruses had previously been studied largely by bulk techniques using very large numbers of virus particles, which yielded averaged results only. When RNA uncoating from HRV or poliovirus virions was triggered in averaging experiments, a populated intermediate state (A particle) was detected that had lost VP4 subunits and externalized VP1 Nts. In the second step, RNA was released from those intermediate particles, which generally became empty capsids.^[23,79,80]

The use of AFM and an SMFS procedure to analyze virus uncoating has of course its own limitations. For example, it is unclear to what extent the vectorial application of mechanical

force may adequately mimic the supply of energy by biochemical means during infection *in vivo*. Careful analysis of the raw data is important to differentiate between real conformational transitions of the viral particle and technical issues (such as particle movements and tip slippage). The model applied did not consider the re-internalization of the RNA molecule, which is unlikely but cannot be completely discarded. Despite the shortcomings, the SMFS procedure implemented in this study did provide additional insights into HRV uncoating that could not be obtained using averaging approaches, as discussed next.

At the single-particle level, the enterovirus uncoating steps identified in bulk experiments are not as clear-cut, and the process appears to involve a continuum of transient intermediates. A bulk approach^[80] as well as AFM imaging^[61] had already shown that acidification *in vitro* can sometimes lead to partial, and not total, RNA egress from HRV virions. Cryo-EM analysis of the poliovirus end-state empty capsid (80 S) indicated that, for a small fraction of the viral particles, RNA was present on both the outside and the inside of the capsid, and suggested a gradual release of the RNA molecule.^[28] Likewise, in the present study application of a force gradient to individual HRV virions elicited a structural transition that resulted in heterogeneous virus particles in which different lengths of their RNA molecule had been externalized. Moreover, single-particle force spectroscopy allowed a quantitative kinetic analysis of the transition that resulted in the subsequent, gradual release of the RNA molecule, and provided an estimation of the fraction of RNA extruded from individual virus particles under increasing mechanical load.

A question that remains to be addressed concerns the regions of the virion and the specific protein–protein or protein–RNA interactions that are involved in the destabilization of the virion and the release of the RNA under mechanical force. In the HRV atomic structures determined to date,^[81,82] a few capsid–RNA interactions were revealed, but most of the RNA molecule could not be traced. If an atomic structure of the HRV virion could be obtained in which the RNA structure and the RNA–capsid interactions are detailed, steered molecular dynamics simulations and mutational analysis could be performed to investigate the structural determinants of HRV destabilization under load. Such studies could provide important additional insights on viral genome uncoating.

The results of the present single-particle study, building on those of previous studies using mainly bulk approaches^[5,8,21,22,25,27,29,30,79–82] provide experimental support for a model of HRV genome uncoating as a stochastic process governed by a moderate free energy barrier. The RNA molecule in the HRV virion is known to be non-covalently bound to the capsid inner wall.^[81,82] The viral RNA–capsid interactions contribute to strengthen the virion (this study), which remains in a relatively stable (basal) conformational state. Thermal energy, and the additional energy provided by receptor binding, acidification, or heating,^[5,8,21,22,25] or application of mechanical force (this study), will weaken the VP4–capsid and RNA–capsid interactions^[81,82] and destabilize the viral particle relative to its basal state. Such weakening was revealed in this study by the observation that, even though all or a part of the RNA molecule is still inside those particles, the low force required to break an intermediate viral particle (the particle that resulted from a

high-force event) was the same than that required to break a capsid completely devoid of RNA.

The structurally weakened intermediate viral particles are more prone than basal-state virions to the opening of fractures or holes at the protein–protein interfaces, and the RNA in them has been unbound from the capsid.^[81,82] Both effects will facilitate the gradual externalization of an increasingly larger segment of the RNA molecule. In some intermediate particles, the exposed RNA segment may be hydrolyzed by ubiquitous RNases, or the RNA molecule may become fully released too early, rendering in both cases non-infectious virus particles. This effect will contribute to explain the well-known facts that i) typically, only a fraction of the viral particles in a population are infectious;^[83] and ii) some empty capsids are present in intact virion populations. Only those intermediate particles that will still carry (partly inside and partly outside) an undegraded RNA molecule can be infectious. Given enough time, even without an additional energy supply, the RNA molecule could be completely released from the intermediate particle by diffusion, leaving an empty capsid behind. However, the timely release in HRV-infected cells of the full-length RNA molecule may still require some promoting factor (e.g., acidification in the endosomes).

To recapitulate, HRV populations may be physically heterogeneous and include different proportions of viral particles in different stages of the uncoating process. In view of this heterogeneity, when a single HRV particle enters a host cell during initiation of infection one may find: i) an infectious virion; ii) an infectious particle carrying partially exposed but still intact RNA; iii) a non-infectious particle in which a part of the externalized RNA was degraded; iv) a noninfectious empty capsid. This scenario introduces an important element of unpredictability in viral infection that is usually not contemplated. When a single HRV particle enters a host cell, viral multiplication may succeed only if i) that particular particle happens to have a full-length RNA molecule still protected inside; and ii) the RNA molecule happens to be fully released while being inserted into the endosome membrane for translocation to the cytosol, without being exposed for too long to the environment. As only very few cells in the host organism may initially be infected, the outcome of the infection process will be uncertain.

Bulk experiments had shown that certain HRV capsid pocket-binding compounds that inhibit viral infection stabilized the virion against disruption by heat denaturation.^[84] Using SMFS to specifically probe the transition that facilitated the release of the RNA molecule from single HRV virions, we found that both pocket-binding anti-HRV drugs (pirodavir and pleconaril) and also a deleterious capsid mutation (R3143A) decreased the transition rate. Moreover, a fair quantitative relationship was found between the rate constant for that transition in the absence or presence of drugs or mutation (R3143A), and virus infectivity. The structural effect of this mutation on the virus could be expected to be quite different from those of the tested drugs because: i) the mutation involves a permanent, not a transient modification of the viral particle; and ii) the mutated residue is located at the interface between capsid subunits, close to the RNA exit site but far from the drug-binding capsid pockets. Thus, the correlation found between reaction rate and infectious titer when such different modifications were compared suggests a true linkage between the free energy barrier of the transition that facilitated RNA

release and HRV infectivity. It also indicated that the antiviral effect of pocket-binding drugs is at least partly mediated by its effect on the kinetics of the structural transition involved in genome uncoating.

In a previous study, we had shown that capsid pocket-binding drugs including pleconaril, and also certain pocket-filling mutations, increase the overall mechanical stiffness of the HRV virion. Moreover, we found a clear quantitative correlation between virion stiffening and impaired infectivity by drug binding or capsid mutation.^[60] Taken together, these results and those of the present study indicate that, from a fundamental physics perspective, capsid pocket-binding drugs may at least partly exert their antiviral effect by stiffening the HRV virion; and that the reduced deformability of the virion may lead to some increase in the free energy barrier for the transition that facilitates RNA release, impairing genome uncoating and, as a consequence, impairing viral infection.

Finally, it must be stressed that SMFS allowed also the clear differentiation and quantitative kinetic characterization of two different transitions in a virus particle. SMFS may be used to identify and analyze the kinetics of any structural transition in a virus particle that can be detected as a specific force-related event, separate from other events in an FR experiment. The SMFS procedure implemented here opens up many possibilities for quantifying at the single-molecule level biologically relevant individual reactions during the complex infectious cycle of different viruses. It may also be used to analyze the kinetics at the single-molecule level of structural transitions of large biomolecular complexes in general.

4. Experimental Section

Production and Purification of HRV-B14 Virions: The procedure used to obtain highly pure HRV-B14 virions was previously described.^[60] Briefly, an HRV-B14 infectious DNA clone was transcribed in vitro by using T7 RNA polymerase following manufacturer instructions (Promega) and electroporated in HeLa-H1 cells by a single pulse (980 V, 25 μ F and maximum resistance) with a Gene Pulser II (BioRad). Transfected cells were grown in Petri dishes at 35 °C until a complete cytopathic effect was reached (usually after 72 h post electroporation). Cell culture supernatants were collected, frozen, and thawed three times, and progeny virions were purified essentially as described previously.^[60] Virus suspensions were placed on top of a sucrose cushion (30% w/v sucrose, 1% sarcosyl, 0.1% mercaptoethanol in PBS) and centrifuged in an SW40 rotor (Beckman) at 40 000 rpm for 130 min at 4 °C. The pellet was thoroughly resuspended in PBS containing 0.01% bovine serum albumin, and subsequently deposited on top of a 7.5–45% sucrose gradient in PBS and centrifuged in the same rotor at 40 000 rpm for 110 min at 4 °C. Fractions containing viral proteins were identified by SDS-PAGE. Fractions containing virions were pooled and thoroughly dialyzed against PBS. The purity of virion suspensions was analyzed by SDS-PAGE and negative staining electron microscopy. Purified virion suspensions were concentrated by ultrafiltration (Amicon Ultracel 100K) at 4 °C, and stored at 4 °C until use.

Production and Purification of Empty Capsids: Capsids (80 S) of HRV-B14 were prepared by an adaptation of previously published protocols.^[81,85] A purified virion (100 μ l) preparation in PBS was dialyzed against 0.1 M sodium phosphate buffer pH = 6. Dialyzed samples were incubated at 45 °C for 15 min, loaded on top of a 16–33% sucrose gradient in PBS, and centrifuged in a SW40 rotor at 40 000 rpm for 85 min at 4 °C. Minute virus of mice capsids (sedimentation coefficient 80S), were used as a marker. Individual fractions of 450 μ l were collected and separately dialyzed against PBS. The presence and integrity of empty HRV-B14

capsids in the fractions with the expected sedimentation coefficient (80 S) were estimated by negative staining electron microscopy.

Electron Microscopy: HRV-B14 virions and empty capsids were deposited on ionized Formvar/carbon-coated copper grids (Electron Microscopy Sciences). Particles were left to absorb for 4 min at room temperature (r.t.) and washed three times for 30 s each. The samples were stained for 45 s at r.t. in 2% (w/v) of either uranyl acetate or phosphotungstic acid (Electron Microscopy Sciences) and visualized using an electron microscope (JEM-1010 (JEOL) equipped with a TemCam F416 (TVIPS) CMOS camera, JEM1400 Flash (JEOL) equipped with a Oneview (Gatan) CMOS camera. Image magnification ranged from 12000X to 50000X.

Surface Functionalization for AFM Experiments: In FR spectroscopy experiments forces applied to HRV virions reached values of 5 nN. Thus, the strong attachment of the virions to a solid surface was promoted through covalent bonding. To this end, functionalization protocols previously described^[86–88] were adapted as follows. Rounded glass coverslips (ϕ 24 mm, Thermo Scientific) were cleaned by sonication for 10 min in a 15 M KOH solution at r.t. They were rinsed with deionized water, and sonication was repeated two more times (10 min each), and dried at 110 °C for 20 min. Coverslips were functionalized by immersing them for 2 min in a 2% aminopropyltriethoxysilane (APTES) solution in chloroform. APTES excess was removed by coverslip immersion into chloroform for 2 min. Then, the treated coverslips were covered with 50 μ l of a 0.5 mM glutaraldehyde solution for 30 min, after which the liquid was removed and the coverslips were dried in a fume hood. Functionalized coverslips were stored in a sealed box at r.t. for one week at most.

AFM Imaging: Purified virion or capsid samples were diluted in PBS enough to obtain well-separated particles on the functionalized solid surface. For virus particle imaging by AFM, a 20 μ l drop of the sample was placed on the functionalized surface and left undisturbed for at least 30 min at r.t. AFM cantilevers RC800PSA (Olympus; nominal elastic constant $k_c = 0.05$ N m⁻¹) were generally used. Cantilevers qp-BioAC (Nanosensors; nominal elastic constant $k_c = 0.06$ N m⁻¹) were used in some experiments, including those involving combined AFM-TIRF microscopy. Imaging of isolated HRV virions in an AFM instrument (Nanotec Electrónica S.A.) was carried out in liquid in jumping mode, and controlled by WSxM software.^[89] At the beginning of each experiment, the actual elastic constant of the cantilever in use was determined by the Sader method.^[90] Normal force during imaging was \sim 10–80 pN. AFM images were processed with WSxM software.^[89]

FR Spectroscopy by AFM and Data Analysis: In order to be able to accelerate the kinetics of the HRV RNA uncoating process the FR protocol implemented in the WSxM software^[89] (which controls the AFM) was used. In this protocol, the force applied to the sample could be increased linearly as a function of time. A determined time dependency of the force exerted over the sample was set and the corresponding vertical displacements of the piezoelectric device (Z-displacements) were determined.^[70] The Z-displacement values thus obtained were transformed to AFM tip-sample separation (TSS) values by subtracting the cantilever deflection. The setup yielded, as it should, a constant TSS at the end of the recording, when the cantilever tip and sample were in intimate contact, entering the incompressible range. This AFM-based FR protocol was used to record the force and TSS at which a concrete physical event occurred (e.g., a structural transition of the viral particle or RNA exit from the particle). Then, the probability of observing that event as a function of the applied force was obtained by integrating the corresponding force histogram. A two-state kinetic model with a linear force increase (constant force rate) was assumed, and the probability of the observed process P_u was calculated by using the following analytical expression that was derived by Schlierf et al. (2004)^[68]

$$P_u = 1 - \exp \left\{ \frac{\alpha_0 k_B T}{r \cdot x^\ddagger} \left[1 - \exp \left(\frac{F \times x^\ddagger}{k_B T} \right) \right] \right\} \quad (1)$$

Experimental values were fitted to Equation (1) using the following fixed data: $k_B T = 4.1$ pN nm; force rates $r = 0.72 \pm 0.05$, 0.86 ± 0.06 , 1.0 ± 0.1 or 1.9 ± 0.2 nN s⁻¹. The independent variable was the applied force F . The fitting yielded the distance to the energy barrier (x^\ddagger) and the rate constant at zero force (α_0) for the physical event being studied.

The activation energy ΔG^\ddagger associated with the physical event at an absolute temperature T was determined by using the following expression and assuming a natural frequency of the process $\nu = 5 \times 10^{11} \text{ s}^{-1}$ (estimated from ref. [23] for a similar transition of poliovirus, another enterovirus):

$$\Delta G = -k_B T \ln \left(\frac{\alpha_0}{\nu} \right) \quad (2)$$

Combined AFM and Fluorescence Microscopy: For correlative AFM-TIRF microscopy analysis, thick sheets of cleaved mica were glued with optical adhesive (NOA 63, Norland) on clean glass coverslips and cured under a UV lamp for at least 1 h. The cured substrates were cleaved again and a 20 μL drop of 50 mM Tris-HCl buffer pH = 7.6, containing 5 mM NiCl_2 and fluorescent beads (1:250 dilution of a 0.1 μM suspension of Tetraspeck Microspheres, Invitrogen) was added and incubated for 15 min at r.t. After washing with the same buffer, a 40 μL drop of a virion suspension at adequate concentration was deposited on the substrate and incubated for 30 min at r.t. Nonadsorbed particles were removed by rinsing three times with buffer. Then, a 1 μL drop of a 1:100 stock solution of fluorophore (Ribogreen, Invitrogen) solution was added. A custom-built inverted fluorescence microscope (TIRFM) coupled to an AFM instrument was used.^[73] Fluorophore excitation was done using a laser diode (Nichia, Japan) of 488 nm wavelength. Dichroic and emission filters were from Semrock (USA), and all optomechanical parts and lenses were manufactured by Thorlabs (USA). Fluorescence intensity was recorded using a Neo 5.5 sCMOS camera (Andor, UK) by setting the exposure time to 0.1 s. Individual particles were then localized and imaged by AFM in jumping mode^[89] under forces ranging from 10 to 50 pN. Before a FR indentation, fluorescence images were obtained in order to assess that there were no fluorescent spots close to the particle to be indented. A force ramp was then recorded as described above, after which additional fluorescence images were acquired to detect whether a new fluorescence spot had appeared at the position where the indented viral particle was located.

Molecular volumes for viral proteins and nucleic acid molecules: Protein volume was estimated by using the following equation:^[75]

$$V_p = \frac{M_w}{N_A} \times (V_p + d \times V_w) \quad (3)$$

where M_w is the molecular weight, N_A is Avogadro's number, V_p and V_w are the protein and water-specific volumes (0.74 and 1 $\text{cm}^3 \text{ g}^{-1}$, respectively) and d is the extent of protein hydration (0.4 mol $\text{H}_2\text{O}/\text{mol}$ protein). The molecular volumes thus calculated for HRV capsid proteins VP1 (33 kDa), VP2 (28 kDa), VP3 (26 kDa) and VP4 (7 kDa) were ≈ 40 , 34, 32 and 8 nm^3 , respectively. Hydrated RNA volume was estimated by extrapolating experimental values obtained for hydrated single-stranded DNA.^[74] The volume of the HRV genomic RNA (7.2 kilobases) thus estimated was $\approx 9300 \text{ nm}^3$.

Supporting Information

Supporting Information is available from the Wiley Online Library or from the author.

Acknowledgements

The authors gratefully acknowledge I. Horcas for implementing the FR protocol in the AFM software and A. Rodríguez-Huete for initial preparation of HRV virions. This work was funded by grants from MICINN/FEDER EU to M.G.M. (RTI2018-096635-B-I00 and PID2021-126973OB-I00) or P.J.P. (FIS2017-89549-R, FIS2017-90701-REDT and PID2021-126608OB-I00); a grant from the Human Frontiers Science Program to P.J.P. (HFSP0 RGP0012/2018); institutional grants from the Severo Ochoa Program for Centers of Excellence in R&D (CEX2021-00154-S) and Fundación Ramón Areces to the Centro de Biología Molecular "Severo Ochoa" (UAM-CSIC);

and an institutional grant from the María de Maeztu Program for Units of Excellence in R&D (MDM-2014-0377) to the Centro de Investigación de Física de la Materia Condensada (UAM). M.G.M. is an associate member of the Institute for Biocomputation and Physics of Complex Systems, Zaragoza, Spain.

Conflict of Interest

The authors declare no conflict of interest.

Author Contributions

A.V. performed the experiments and analyzed data; A.V. and K.S. performed combined AFM-fluorescence experiments; J.C.G. and L.V. obtained biological materials; A.V., M.G.M., K.S., and P.J.P. interpreted results; M.G.M. and A.V. designed the study and wrote the paper.

Data Availability Statement

The data that support the findings of this study are available from the corresponding author upon reasonable request.

Keywords

antiviral drug, atomic force microscopy, capsid, conformational transition, infections, rhinovirus, virus

Received: June 5, 2023
Revised: September 26, 2023
Published online:

- [1] J. E. Johnson, *Adv. Protein Chem.* **2003**, 64, 197.
- [2] M. B. Sherman, H. Q. Smith, T. J. Smith, *Viruses* **2020**, 12, 618.
- [3] (Eds.: M. G. Rossmann, V. B. Rao), *Viral Molecular Machines*, Springer, New York, USA, **2012**.
- [4] (Ed.: M. G. Mateu), *Structure and Physics of Viruses*, Springer, Dordrecht, Netherlands, **2013**.
- [5] J. M. Casasnovas, in *Structure and Physics of Viruses*, vol. 68, Springer, Dordrecht, Netherlands, **2013**, p. 441.
- [6] Y. Yamauchi, U. F. Greber, *Traffic* **2017**, 17, 569.
- [7] U. F. Greber, J. W. Flatt, *Annu. Rev. Virol.* **2019**, 6, 177.
- [8] T. J. Tuthill, E. Groppe, J. M. Hogle, D. J. Rowlands, *Curr. Top. Microbiol. Immunol.* **2010**, 343, 43.
- [9] (Eds.: E. Ehrenfeld, E. Domingo, R. P. Roos), *The Picornaviruses*, ASM Press, Washington DC, **2010**.
- [10] M. B. Hersenson, in *The Picornaviruses* (Eds.: E. Ehrenfeld, E. Domingo, R. P. Roos), ASM Press, Washington DC, **2010**, pp. 369–381.
- [11] G. Gabutti, E. d'Anchera, F. Sandri, M. Savio, A. Stefanati, *Infect. Dis. Ther.* **2020**, 9, 241.
- [12] S. E. Jacobs, D. M. Lamson, K. S. George, T. J. Walsh, *Clin. Microbiol. Rev.* **2013**, 26, 135.
- [13] E. Kieninger, F. Singer, C. Tapparel, M. P. Alves, P. Latzin, H.-L. Tan, C. Bossley, C. Casaulta, A. Bush, J. C. Davies, L. Kaiser, N. Regamey, *Chest* **2013**, 143, 782.
- [14] A. I. Ritchie, H. A. Farne, A. Singanayagam, D. J. Jackson, P. Mallia, S. L. Johnston, *Ann. Am. Thorac. Soc.* **2015**, 12, S115.
- [15] S.-R. Shih, S.-J. Chen, G. H. Hakmelah, H.-J. Liu, C.-T. Tseng, K.-S. Shia, *Med. Res. Rev.* **2004**, 24, 449.

- [16] A. M. D. Palma, I. Vliegen, E. De Clercq, J. Neyts, *Med. Res. Rev.* **2008**, *28*, 823.
- [17] H. J. Thibaut, A. M. De Palma, J. Neyts, *Biochem. Pharmacol.* **2012**, *83*, 185.
- [18] S. P. Swain, S. Mohanty, *Chem. Med. Chem.* **2019**, *14*, 291.
- [19] M. G. Rossmann, E. Arnold, J. W. Erickson, E. A. Frankenberger, J. P. Griffith, H.-J. Hecht, J. E. Johnson, G. Kamer, M. Luo, A. G. Mosser, R. R. Rueckert, B. Sherry, G. Vriend, *Nature* **1985**, *317*, 145.
- [20] P. Jiang, Y. Liu, H.-C. Ma, A. V. Paul, E. Wimmer, *Microbiol. Mol. Biol. Rev.* **2014**, *78*, 418.
- [21] M. A. McKinlay, D. C. Pevear, M. G. Rossmann, *Annu. Rev. Microbiol.* **1992**, *46*, 635.
- [22] M. G. Rossmann, *Protein Sci.* **1994**, *3*, 1712.
- [23] S. K. Tsang, P. Danthi, M. Chow, J. M. Hogle, *J. Mol. Biol.* **2000**, *296*, 335.
- [24] J. M. Hogle, *Annu. Rev. Microbiol.* **2002**, *56*, 677.
- [25] R. Fuchs, D. Blaas, *Rev. Med. Virol.* **2010**, *20*, 281.
- [26] C. Xiao, M. A. McKinlay, M. G. Rossmann, in *Structural Virology* (Eds: M. Agbandje-McKenna, R. McKenna), RSC Publishing, Cambridge **2011**, pp. 319-337.
- [27] D. Blaas, *Wien. Med. Wochenschr.* **2016**, *166*, 211.
- [28] M. Bostina, H. Levy, D. J. Filman, J. M. Hogle, *J. Virol.* **2011**, *85*, 776.
- [29] D. Garriga, A. Pickl-Herk, D. Luque, J. Wruss, J. R. Castón, D. Blaas, N. Verdager, *PLoS Pathog.* **2012**, *8*, e1002473.
- [30] Y. Dong, Y. Liu, W. Jiang, T. J. Smith, Z. Xu, M. G. Rossmann, *Proc. Natl. Acad. Sci. USA* **2017**, *114*, 8017.
- [31] J. R. Moffitt, Y. R. Chemla, S. B. Smith, C. Bustamante, *Annu. Rev. Biochem.* **2008**, *77*, 205.
- [32] Y. R. Chemla, D. E. Smith, *Adv. Exp. Med. Biol.* **2012**, *726*, 549.
- [33] J. R. Arias-Gonzalez, in *Structure and Physics of Viruses*, Springer, Dordrecht, Netherlands, **2013**, *68*, 273.
- [34] M. Marchetti, G. Wuite, W. Roos, *Curr. Opin. Virol.* **2016**, *18*, 82.
- [35] P. J. de Pablo, *Adv. Virus Res.* **2019**, *105*, 161.
- [36] W. H. Roos, R. Bruinsma, G. J. L. Wuite, *Nat. Phys.* **2010**, *6*, 733.
- [37] P. G. Stockley, R. Twarock (eds.), *Emerging Topics in Physical Virology*, Imperial College Press, London, **2010**.
- [38] (Ed.: U. F. Greber), *Physical Virology*, Springer, Cham, Switzerland **2019**.
- [39] P. Buzón, S. Maity, W. H. Roos, *Wiley Interdiscip. Rev.: Nanomed. Nanobiotechnol.* **2020**, e1613.
- [40] D. E. Smith, S. J. Tans, S. B. Smith, S. Grimes, D. L. Anderson, C. Bustamante, *Nature* **2001**, *413*, 748.
- [41] Y. R. Chemla, K. Aathavan, J. Michaelis, S. Grimes, P. J. Jardine, D. L. Anderson, C. Bustamante, *Cell* **2005**, *122*, 683.
- [42] C. M. Knobler, W. M. Gelbart, *Annu. Rev. Phys. Chem.* **2009**, *60*, 367.
- [43] T. Liu, U. Sae-Ueng, D. Li, G. C. Lander, X. Zuo, B. Jönsson, D. Rau, I. Shefer, A. Evilevitch, *Proc. Natl. Acad. Sci. USA* **2014**, *111*, 14675.
- [44] M. S. Z. Kellermayer, Z. Vörös, G. Csík, L. Herényi, *Nanoscale* **2018**, *10*, 1898.
- [45] C. Rankl, F. Kienberger, L. Wildling, J. Wruss, H. J. Gruber, D. Blaas, P. Hinterdorfer, *Proc. Natl. Acad. Sci. USA* **2008**, *105*, 17778.
- [46] A. Ortega-Esteban, K. Bodensiek, C. San Martín, M. Suomalainen, U. F. Greber, P. J. De Pablo, I. A. T. Schaap, *ACS Nano* **2015**, *9*, 10571.
- [47] U. F. Greber, *J. Virol.* **2016**, *90*, 3802.
- [48] A. Ortega-Esteban, G. N. Condezo, A. J. Pérez-Berná, M. Chillón, S. J. Flint, D. Reguera, C. San Martín, P. J. De Pablo, *ACS Nano* **2015**, *9*, 10826.
- [49] P. J. De Pablo, C. San Martín, *Curr. Opin. Virol.* **2022**, *52*, 112.
- [50] M. Medrano, M. Á. Fuertes, A. Valbuena, P. J. P. Carrillo, A. Rodríguez-Huete, M. G. Mateu, *J. Am. Chem. Soc.* **2016**, *138*, 15385.
- [51] R. F. Garmann, A. M. Goldfain, V. N. Manoharan, *Proc. Natl. Acad. Sci. USA* **2019**, *116*, 22485.
- [52] A. Valbuena, S. Maity, M. G. Mateu, W. H. Roos, *ACS Nano* **2020**, *14*, 8724.
- [53] C. Bustamante, *Protein Sci.* **2004**, *13*, 3061.
- [54] I. L. Ivanovska, P. J. De Pablo, B. Ibarra, G. Sgalari, F. C. Mackintosh, J. L. Carrascosa, C. F. Schmidt, G. J. L. Wuite, *Proc. Natl. Acad. Sci. USA* **2004**, *101*, 7600.
- [55] M. Castellanos, R. Pérez, C. Carrasco, M. Hernando-Pérez, J. Gómez-Herrero, P. J. De Pablo, M. G. Mateu, *Proc. Natl. Acad. Sci. USA* **2012**, *109*, 12028.
- [56] M. G. Mateu, *Virus Res.* **2012**, *168*, 1.
- [57] P. J. de Pablo, M. G. Mateu, in *Structure and Physics of Viruses*, Springer, Dordrecht, Netherlands, **2013**, *68*, 519.
- [58] A. Llauró, B. Schwarz, R. Koliyatt, P. J. De Pablo, T. Douglas, *ACS Nano* **2016**, *10*, 8465.
- [59] P. J. P. Carrillo, M. Medrano, A. Valbuena, A. Rodríguez-Huete, M. Castellanos, R. Pérez, M. G. Mateu, *ACS Nano* **2017**, *11*, 2194.
- [60] A. Valbuena, A. Rodríguez-Huete, M. G. Mateu, *Nanoscale* **2018**, *10*, 1440.
- [61] F. Kienberger, R. Zhu, R. Moser, D. Blaas, P. Hinterdorfer, *J. Virol.* **2004**, *78*, 3203.
- [62] K. Strobl, M. G. Mateu, P. J. De Pablo, *Virology* **2023**, *581*, 1.
- [63] A. Fersht, *Structure and Mechanism in Protein Science: A Guide to Enzyme Catalysis and Protein Folding*, World Scientific, New Jersey **1999**.
- [64] M. Carrion-Vazquez, A. F. Oberhauser, S. B. Fowler, P. E. Marszalek, S. E. Broedel, J. Clarke, J. M. Fernandez, *Proc. Natl. Acad. Sci. USA* **1999**, *96*, 3694.
- [65] F. Oesterhelt, D. Oesterhelt, M. Pfeiffer, A. Engel, H. E. Gaub, D. J. Mu?ller, *Science* **2000**, *288*, 143.
- [66] A. F. Oberhauser, P. K. Hansma, M. Carrion-Vazquez, J. M. Fernandez, *Proc. Natl. Acad. Sci. USA* **2001**, *98*, 468.
- [67] C. Bustamante, Y. R. Chemla, N. R. Forde, D. Izhaky, *Annu. Rev. Biochem.* **2004**, *73*, 705.
- [68] M. Schlierf, H. Li, J. M. Fernandez, *Proc. Natl. Acad. Sci. USA* **2004**, *101*, 7299.
- [69] A. Borgia, P. M. Williams, J. Clarke, *Annu. Rev. Biochem.* **2008**, *77*, 101.
- [70] A. Valbuena, J. Oroz, R. Hervás, A. M. Vera, D. Rodríguez, M. Menéndez, J. I. Sulkowska, M. Cieplak, M. Carrión-Vázquez, *Proc. Natl. Acad. Sci. USA* **2009**, *106*, 13791.
- [71] M. Carrillo-Tripp, C. M. Shepherd, I. A. Borelli, S. Venkataraman, G. Lander, P. Natarajan, J. E. Johnson, C. L. Brooks, V. S. Reddy, *Nucleic Acids Res.* **2009**, *37*, D436.
- [72] E. A. Hewat, D. Blaas, *J. Virol.* **2004**, *78*, 2935.
- [73] K. Strobl, E. Selivanovitch, P. Ibanez-Freire, F. Moreno-Madrid, I. A. T. Schaap, R. Delgado-Buscalioni, T. Douglas, P. J. De Pablo, *Small* **2022**, *18*, 2200059.
- [74] M. E. Fuentes-Perez, M. S. Dillingham, F. Moreno-Herrero, *Methods* **2013**, *60*, 113.
- [75] S. W. Schneider, J. Lärmer, R. M. Henderson, H. Oberleithner, *Pflügers Arch.* **1998**, *435*, 362.
- [76] M. T. Heise, *H.W. Virgin in Fields Virology*, 6th ed. (Eds: D. M. Knipe, P. M. Howley), Lippincott, Williams & Wilkins, Philadelphia, **2013**, pp. 254–285.
- [77] E. Domingo, *Virus as Populations*, Elsevier, Amsterdam **2016**.
- [78] C. Carrasco, M. Douas, R. Miranda, M. Castellanos, P. A. Serena, J. L. Carrascosa, M. G. Mateu, M. I. Marqués, P. J. De Pablo, *Proc. Natl. Acad. Sci. USA* **2009**, *106*, 5475.
- [79] J. M. Casasnovas, T. A. Springer, *J. Virol.* **1994**, *68*, 5882.
- [80] S. Harutyunyan, H. Kowalski, D. Blaas, *J. Virol.* **2014**, *88*, 6307.
- [81] A. Pickl-Herk, D. Luque, L. Vives-Adrián, J. Querol-Audí, D. Garriga, B. L. Trus, N. Verdager, D. Blaas, J. R. Castón, *Proc. Natl. Acad. Sci. USA* **2013**, *110*, 20063.

- [82] D. Hřebík, T. Füzik, M. Gondová, L. Smerdová, A. Adamopoulos, O. Sedo, Z. Zdráhal, P. Plevka, *Proc. Natl. Acad. Sci. USA* **2021**, 118, e2024251118.
- [83] P. J. Klasse, *Prog. Mol. Biol. Transl. Sci.* **2015**, 129, 285.
- [84] V. M. Okun, S. Nizet, D. Blaas, E. Kenndler, *Electrophoresis* **2002**, 23, 896.
- [85] K. Lonberg-Holm, J. Noble-Harvey, *J. Virol.* **1973**, 12, 819.
- [86] P. Facci, D. Alliata, L. Andolfi, B. Schnyder, R. Kötz, *Surf. Sci.* **2002**, 504, 282.
- [87] H. Wang, R. Bash, J. G. Yodh, G. L. Hager, D. Lohr, S. M. Lindsay, *Biophys. J.* **2002**, 83, 3619.
- [88] D. Lohr, R. Bash, H. Wang, J. Yodh, S. Lindsay, *Methods* **2007**, 41, 333.
- [89] I. Horcas, R. Fernández, J. M. Gómez-Rodríguez, J. Colchero, J. Gómez-Herrero, A. M. Baro, *Rev. Sci. Instrum.* **2007**, 78, 13705.
- [90] J. E. Sader, J. W. M. Chon, P. Mulvaney, *Rev. Sci. Instrum.* **1999**, 70, 3967.